Effects of Radiation and Turbulence on the Diabatic Heating and Water Budget of the Stratiform Region of a Tropical Cloud Cluster

DEAN D. CHURCHILL* AND ROBERT A. HOUZE, JR.

Department of Atmospheric Sciences, University of Washington, Seattle, Washington

(Manuscript received 31 July 1989, in final form 19 October 1990)

ABSTRACT

A two-dimensional, kinematic model, incorporating ice- and water-cloud microphysics, visible and infrared radiation, and convective adjustment, is used to diagnose the thermodynamic, water vapor, and hydrometeor fields of the stratiform clouds associated with a mesoscale tropical cloud cluster. The goal is to determine the relative contributions of radiation, microphysics, and turbulence to diabatic heating, and the effects that radiation has on the water budget of the cluster in the absence of dynamical interactions.

The model was initialized with observed steady-state vertical and horizontal wind speeds, and thermodynamic fields corresponding to the stratiform region of a GATE tropical squall line. The wind field is held constant while thermodynamic and hydrometeor fields adjust to a steady state consistent with the prescribed winds. Advection of hydrometeors into the stratiform region from the convective line located just ahead of the stratiform region was estimated with the aid of a one-dimensional convective model, which indicated the vertical distribution of hydrometeors produced by the convective cells. These hydrometeor distributions were assumed to apply throughout the calculations on the upwind lateral boundary of the stratiform region, which lay just behind the line of convection. Particles produced by convection were thus advected into the stratiform region from this boundary by the prescribed wind field.

During nighttime, energy loss due to infrared flux divergence was balanced by horizontal temperature advection and by vertical eddy flux convergence of moist static energy. The latter occurred when radiative destabilization led to convective overturning in the upper troposphere. Absorption of shortwave radiation by day warmed the cloud over a layer several kilometers deep, but infrared cooling at cloud top was still able to cause destabilization in the top 1 km of cloud.

The solar and infrared radiation did not substantially change the hydrometeor fields, and thus had no effect on the water budget of the precipitating stratiform region. The depth of convective overturning in the upper troposphere was too small and water vapor mixing ratios were too low for radiatively driven convective overturning to affect the water budget of the stratiform precipitation region of the squall line. It was concluded that radiation does not directly affect the water budget of the stratiform region, and any radiative effect on hydrometeors must involve interaction with dynamics.

An incipient anvil (cirrostratus cumulonimbogenitus) was represented by allowing hydrometeors from the convective line to blow off into a region devoid of other cloud or mean vertical air motion. Radiative destabilization maintained saturation in this cloud, and apparently contributed to the longevity of this cirrus, but no precipitation was formed.

1. Introduction

As a result of equatorial field experiments, such as the Global Atmospheric Research Program's Atlantic Tropical Experiment (GATE) in 1974, mesoscale convective systems in the tropics ("cloud clusters") are much better understood. Data from satellites, meteorological radar, specially instrumented ships and aircraft, and special surface observing networks have led to conceptual knowledge of the development and distribution of precipitation, convective and mesoscale air motions, boundary-layer dynamics, and diabatic processes in the troposphere associated with cloud clusters (see reviews by Houze and Betts 1981; Houze and Hobbs 1982; Johnson and Houze 1987; Houze 1989). One aspect of cloud clusters that has not been examined quantitatively, however, is how radiation, turbulence, and dynamical interactions affect the heat and water budgets of a cluster.

Several studies have estimated the radiative forcing in cloud clusters. Webster and Stephens (1980) made preliminary estimates of heating and cooling rates due to infrared and solar flux convergence. A cloud cluster in its mature through dissipating stages has a stratiform cloud deck, which extends vertically from about 5 km to the tropopause (see schematic in Fig. 1 from Houze

* *Current affiliation:* Rosenstiel School of Marine and Atmospheric Science, University of Miami.

Corresponding author address: Dr. Dean Churchill, Rosentiel School of Marine and Atmospheric Sciences, University of Miami, 4600 Rickenbacker Causeway, Miami, FL 33149.

1982), and is active radiatively. Webster and Stephens estimated that the base of this cloud deck is heated by flux convergence of longwave radiation at a rate of about 20° day^{-1}. In the upper troposphere, flux divergence of infrared radiation cools the tops of clouds by 5°–15° day^{-1}. Solar insolation produces heating over a layer of cloud several kilometers deep. Webster and Stephens conjectured that the differential heating between cloud base and top destabilizes the upper troposphere within the cloud deck, and that the resulting convective overturning enhances precipitation.

Ackerman et al. (1988) determined radiative heating rates in tropical cirrostratus. They determined differences in infrared heating between the bases and tops of cirrus clouds, 2 km thick, to be 30°–200° day^{-1}, producing convective instability. They concluded that, on average, infrared radiation heated cirrostratus, since much more infrared radiation from the surface was absorbed than was emitted from the cloud. The differential heating between cloud base and top would cause convective destabilization if the cloud has limited vertical extent and moderate ice-water content.

Houze (1982) employed the profiles of radiative heating of Webster and Stephens (1980) to estimate the contribution of radiation to the vertical profile of diabatic heating in the stratiform portion of cloud clusters. The heating at cloud base was partially offset by cooling due to melting and evaporation of precipitation near cloud base, as indicated by Leary and Houze (1979). Near cloud top, infrared cooling produced net diabatic cooling in a layer of air about 1 km deep, while solar heating and latent heat release produced a maximum of diabatic heating near 9-km altitude.

These studies (Webster and Stephens 1980; Ackerman et al. 1988; Houze 1982) used assumed values of cloud ice content to estimate radiative forcing. It is unclear whether their results would have been different if radiative heating and cooling were allowed to interact with the hydrometeor contents, possibly altering the water budget.

Rutledge (1986) investigated the interactions between mesoscale updraft motion in the stratiform region of the 12 September 1974 GATE squall line and the advection of hydrometeors into the region from convective cells. His simulation, based on composite wind data from soundings, suggested that much of the precipitation in the stratiform region must be generated at mid-to-upper levels by a mesoscale updraft. Since his study did not include radiation, it is possible that convective overturning due to radiative processes could have altered the microphysical structure and contributed to the mesoscale precipitation in the stratiform region.

Dudhia (1989) used a two-dimensional dynamic model to study a winter monsoon cloud cluster and the diurnal precipitation that occurs north of Borneo in association with such clusters. He found that clear-air cooling throughout the troposphere tended to enhance convection. The effect of clear-air cooling on precipitation, which affected the convection primarily, was apparently much greater than any direct effect radiation had on the clouds themselves. With radiation turned off, Dudhia's simulation produced less convection, smaller cirrus shields, and only 36% as much convective and stratiform rainfall. Clear-air cooling without cloud-radiative interactions produced less widespread cirrus.

Chen and Cotton (1988) used a two-dimensional model to simulate a midlatitude mesoscale convective system. They found that infrared radiation increased precipitation at 7-km altitude by 1–2 mm h^{-1} just downwind of the convection. It is not apparent whether the infrared radiation affected the precipitation directly or modified the environment in such a way as to affect the precipitation. They did not investigate whether solar radiation had any effect.

Gamache and Houze (1983) studied the water budget of the 12 September 1974 GATE tropical squall line. Their study did not consider the effects of radiation on microphysics, and it is not known if their results would have been different if radiation were included. Rutledge and Houze (1987) found that the mesoscale updraft in the stratiform region of a midlatitude squall line, combined with seeding from convective cells, produced more precipitation than if either the updraft or the seeding were absent. Again the question arises whether results might have been different if radiation were included in the calculations.

These previous studies leave several questions unresolved. First, what is the direct effect of radiation on the microphysical and thermodynamic structure of the stratiform cloud deck of the cluster, independent of dynamical interactions? Second, to what extent does radiative destabilization generate convective turbulence and small-scale irregularity within the stratiform cloud layer? Third, does such radiative destabilization quantitatively affect the water budget of the stratiform region? Finally, what are the relative magnitudes of solar and infrared radiation and turbulent flux convergence of sensible and latent heat (especially those triggered by radiative destabilization) in the heat budget of the stratiform region and what is the distribution of these heating effects with respect to height? In this study these questions are addressed by setting the objective to quantify the relative importance of solar and infrared heating, convective overturning, and latent heat release on the steady-state energy balance of the stratiform clouds associated with a tropical cloud cluster, and to quantify what effect, if any, radiation acting on the clouds has on the microphysical structure and water budget of the cluster. In the main set of calculations, these aspects are examined within the deep precipitating stratiform clouds of the type found within the core of a major cloud cluster. Second, the interactions of radiation, turbulence, and microphysics are examined

in cirrus clouds of the type found protruding laterally at upper levels from the line of cells prior to the establishment of a well-formed stratiform region.

The GATE squall line of 12 September 1974 was a well-documented mesoscale system with a steady-state stratiform precipitation region that lasted several hours (Gamache and Houze 1982, 1983, 1985; Rutledge and Houze 1987). Using the set of data from Gamache and Houze (1985), a diagnostic model is employed to represent only the stratiform regions of this cloud system. In this simulation, the influence of the convective cells on the stratiform clouds is controlled through boundary conditions, and the mesoscale airflow in the stratiform region is prescribed, while radiation, microphysics, and turbulence are allowed to interact. Thus, dynamical interactions between radiation and convection are eliminated leaving only the direct effects of radiation on the stratiform clouds. The model, described in more detail below, then allows us to isolate the physics relevant to the questions noted earlier.

2. Model description

The methodology is to use a kinematic, two-dimensional mesoscale model with parameterized ice and water microphysics, parameterized short- and longwave radiative fluxes, and parameterized convective overturning. This model combines the Stephens and Webster (1979) solar and infrared two-stream radiation parameterizations for clouds, a clear-air solar and infrared model (Liou and Ou 1981), the kinematic-microphysical model of Rutledge (1986), and a convective adjustment scheme. Rutledge used a version of the bulk parameterized ice-phase microphysics introduced by Lin et al. (1983) and later refined by Rutledge and Hobbs (1983, 1984) and others. Mesoscale updraft motion and horizontal winds were prescribed and held constant throughout a model run. Water categories of vapor, cloud water, rain, cloud ice, snow, and graupel were parameterized in bulk terms. The model was run for 8 h of simulation, by which time steady-state conditions were obtained, producing two-dimensional fields of hydrometeor content, water vapor mixing ratio, temperature, and diabatic heating consistent with the assumed vertical motion. This model removes dynamical feedbacks between radiation and microphysics in the stratiform region and feedbacks on deep penetrating convection in the environment surrounding the stratiform region. This allows us to assess the role of direct radiative destabilization of the cloud system absent dynamical interactions.

A convective adjustment scheme is used to diagnose steady-state fluxes of latent heat and dry static energy in cloud. Eddy mixing coefficients are deduced, and these determine eddy fluxes of hydrometeors.

The model is initialized with two-dimensional fields of temperature, humidity, pressure, height, and horizontal and vertical wind speed for the GATE squall line studied by Gamache and Houze (1982, 1983, and 1985). Rutledge (1986) has used these data to initialize his three-dimensional microphysical model.

a. Thermodynamic balance

The thermodynamic energy equation for the present two-dimensional model is

$$\frac{\partial S}{\partial t} = -w\frac{\partial S}{\partial z} - u\frac{\partial S}{\partial x} + H_R + H_L + H_E, \quad (1)$$

where $S = C_pT + gz$ is the dry static energy, w is vertical wind speed, u is horizontal wind speed, H_R is radiative heating, H_L is latent heat release due to changes of phase in the microphysical parameterization, and H_E is heating due to eddy flux convergence. The heat sources and sinks are parameterized using the microphysical, radiative, and turbulent schemes described below. In the energy balance simulations presented later, the steady-state magnitudes of these terms will be shown.

The continuity equations for *precipitating* hydrometeor species q_η are given by

$$\frac{\partial q_\eta}{\partial t} = -u\frac{\partial q_\eta}{\partial x} - w\frac{\partial q_\eta}{\partial z} - \frac{\partial}{\partial z}(q_\eta V_f) + S_\eta + F_\eta, \quad (2)$$

where q is hydrometeor mixing ratio, and subscript η can be s for snow, r for rain, and g for graupel. Here V_f is the fallspeed of precipitation, S_η and F_η represent sources and sinks of precipitate η. A similar equation describes the continuity of *nonprecipitating* hydrometeors, where, by virtue of cloud water ($\eta = c$) and cloud ice ($\eta = i$) being suspended in the air, the fallspeed is zero:

$$\frac{\partial q_\eta}{\partial t} = -u\frac{\partial q_\eta}{\partial x} - w\frac{\partial q_\eta}{\partial z} + S_\eta + F_\eta + E_\eta. \quad (3)$$

An eddy flux term, E_η, is added to the nonprecipitating hydrometeor fields. It was assumed that precipitation falls much more quickly than eddy fluxes can transport precipitation, so no eddy fluxes were applied to precipitation fields. This term will be parameterized since the kinematic model does not have information about actual eddy velocities (see below). Equations (2) and (3) determine the mixing ratios of the hydrometeors and water vapor. The latent heat released by changes of phase of water determines the values of H_L in Eq. (1).

b. Radiation

The model incorporates heating and cooling from infrared and solar radiation due to water vapor, carbon dioxide, and ozone. Clear-air infrared cooling was determined using the method of Liou and Ou (1981), which accommodates five spectral bands associated with water vapor, carbon dioxide, and ozone, plus a

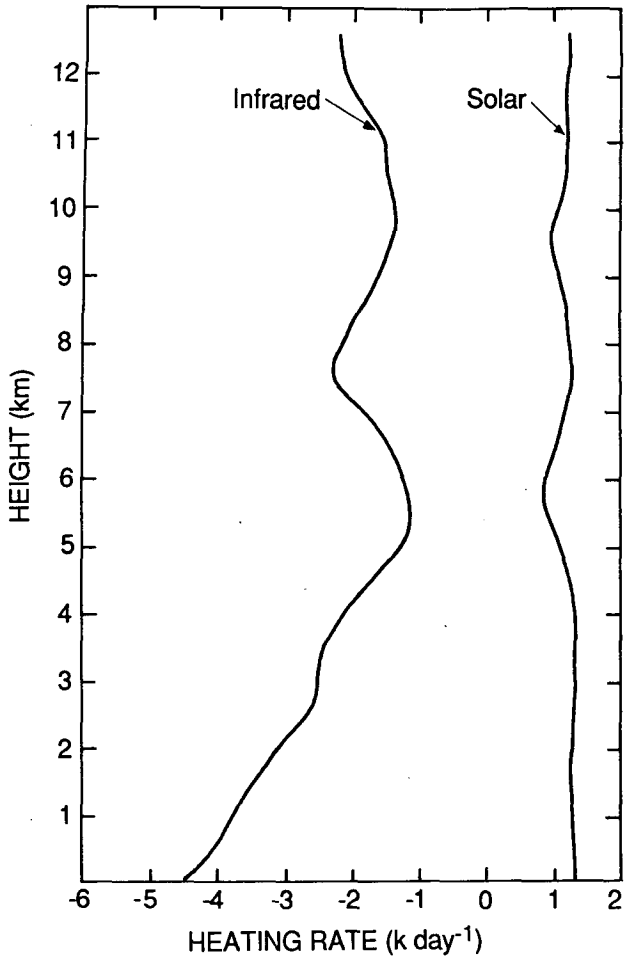

FIG. 1. Clear-air infrared and solar heating rates (K day^{-1}). The *Oceanographer* 1200 UTC sounding on 12 September 1974 provided the temperature and humidity data for the heating rates.

correction for the overlap between the water vapor rotational and carbon dioxide vibrational-rotation bands. Clear-air solar heating was determined using the method of Liou and Sasamori (1975).[1] Figure 1 shows the infrared and solar heating rates using the 1200 UTC *Oceanographer* GATE sounding from 12 September 1974. These rates are prescribed and held fixed during the model simulation for both clear and cloudy skies. Heating and cooling rates in cloud are determined independently and are added to the clear-sky values. This simple method is an approximation but is sufficiently accurate for this study.

Infrared heating and cooling in clouds is accomplished using a two-stream model, as described in the Appendix. The emissivities of clouds were parameterized as a function of hydrometeor pathlength in each vertical grid of the radiation model, according to

$$\epsilon = 1 - e^{-kW} \tag{4}$$

where ϵ is the emissivity, W is the water pathlength (in g m^{-2}), and k (m^2 g^{-1}) is a coefficient. Stephens (1984) reports values of k ranging from 0.056 to 0.096 for cirrus clouds. To tune the radiation model, cloud simulations identical to ones reported in Ackerman et al. (1988) were run using vertical resolution of 200 m. Ackerman et al. computed heating rates in tropical cirrus anvil clouds 2 km thick, with ice-water contents (IWCs) of 0.002, 0.02, and 0.10 g m^{-3}. Using their sounding and cloud definitions, the method obtained good agreement when used with a value of $k = 0.029$. Figure 2 (compare with Fig. 6 of Ackerman et al.) shows the heating rates for variable IWC agree to within 1° day^{-1} for the 0.002 IWC, and except near the lower boundary of the 0.10 g m^{-3} cloud, generally agree to within 2° or 3° day^{-1}. For cloud thickness that ranged from 2 to 10 km, with cloud top at 17 km and with constant IWC of 0.02 g m^{-3}, Fig. 3 shows our heating rates (directly comparable to Fig. 9 of Ackerman et al.) generally agree to within about 1° day^{-1}, with errors of up to about 3° day^{-1} at the bottom of the 10 km thick cloud and at the top of the 2 km thick cloud.

Solar heating rates in cloud were determined using the method of Stephens and Webster (1979), using cloud optical properties for cirrus clouds from Liou and Wittman (1979). To tune this model, the in-cloud heating rates were compared with those of Fig. 12 of Ackerman et al. (1988), using the same solar zenith angle (50°), surface albedo (0.05), and cloud definitions as they did. To improve agreement, the cirrus absorption was multiplied by 0.29. Figure 4 shows our solar heating rates (directly comparable to Fig. 12 of Ackerman et al.) for 2 km thick clouds with varying IWC. Near cloud base, the heating rates differ by about 5° day^{-1}, while in cloud and at cloud top differences were about 2° day^{-1}. Not shown is the curve for 0.002 g m^{-3}, which had a heating rate under 1° day^{-1}, and differed from Ackerman et al. by less than 1° day^{-1}.

The infrared and solar heating rates are considered to be accurate enough to run our diagnostic model for 8 h. In sensitivity tests, where several other values for k were used and the Liou and Wittman optical absorption coefficients were used without modification, the model produced larger rates of heating and cooling in clouds, yet produced the same microphysical results. Hence there is confidence that conclusions drawn in the paper are not sensitive to the tuning of the radiative parameterizations.

c. *Convective adjustment*

In a steady-state stratiform region, convective overturning produces neutral lapse rates and maintains saturated conditions throughout the unstable layer. To simulate this process, when temperature perturbations that resulted from radiative flux convergence produced

[1] A program to compute the clear-air heating and cooling was provided by K.-N. Liou and S.-C. S. Ou.

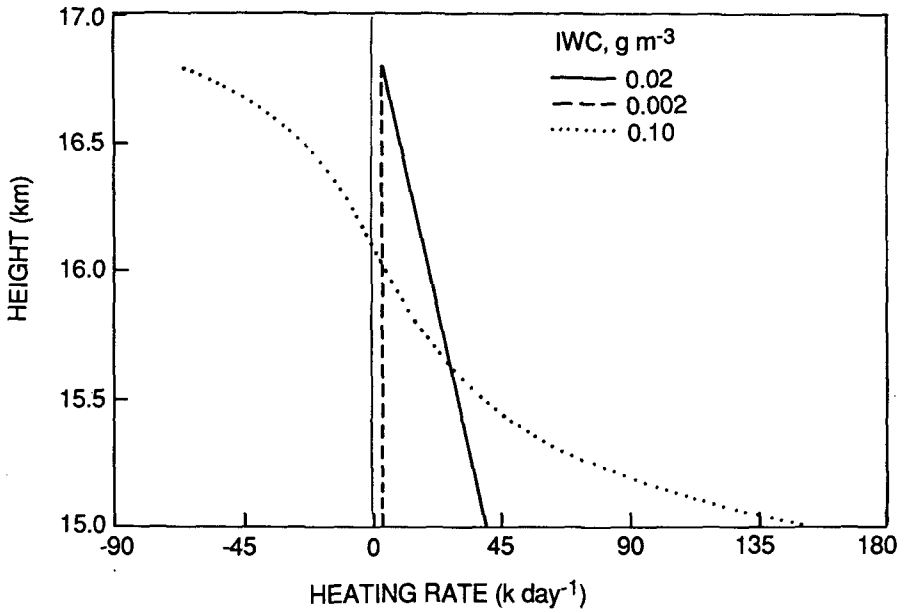

FIG. 2. In-cloud heating rates as a function of height for three ice-water contents: 0.02 g m^{-3} (solid curve), 0.002 g m^{-3} (dashed), and 0.1 g m^{-3} (dotted). Compare with Fig. 6 of Ackerman et al. (1988).

lapse rates that were unstable, the soundings were adjusted to restore stability. The scheme used here, which is similar to those used in some general circulation models (e.g., Manabe et al. 1965), conserves moist static energy. The technique is described in the Appendix. The adjustment process often produces a layer that is supersaturated with respect to ice in the upper troposphere (with respect to water at temperatures above freezing). In this study it was assumed that all vapor in excess of supersaturation in the adjusted layer was deposited on cloud ice when the temperature was below freezing or condensed to cloud water at temperatures at and above freezing. Since radiative destabilization in upper troposphere occurred where much cloud ice was present, the assumption of immediate deposition is probably realistic.

d. Mixing of cloud microphysical fields

Since precipitation is assumed to fall much more quickly than air undergoing turbulent mixing can lift

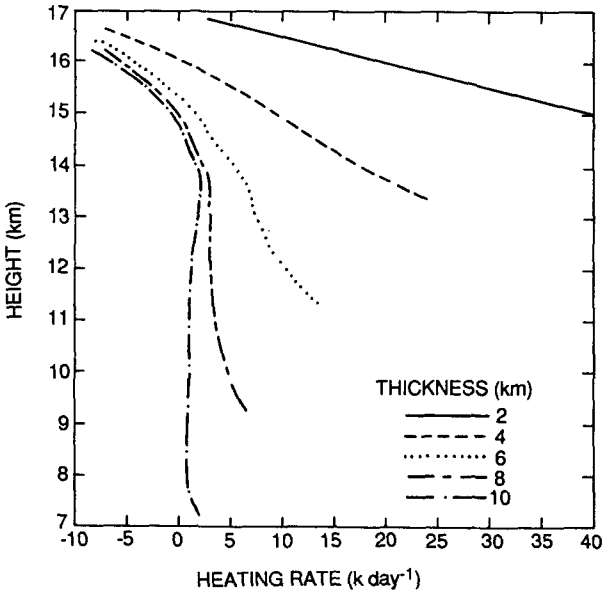

FIG. 3. In-cloud infrared heating rates as a function of height for clouds with a constant ice-water content (IWC) and geometric thicknesses ranging from 2 to 10 km. In all cases cloud top is 17 km. Compare with Fig. 9 of Ackerman et al. (1988).

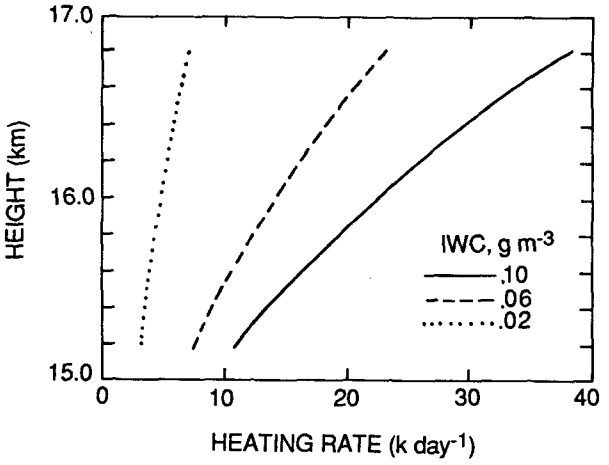

FIG. 4. In-cloud solar heating rates as a function of height for IWCs of 0.02, 0.06, and 0.1 g m^{-3}. The solar zenith angle is 53°. Compare with Fig. 12 of Ackerman et al. (1988).

precipitation, it was not necessary to mix snow and rain. Both cloud water and cloud ice were mixed whenever convective adjustment occurred. Eddy mixing coefficients were determined at each grid point of the model that would provide the same amount of vapor transport as the convective adjustment. Then these coefficients were used in a standard eddy flux scheme to determine the amount of hydrometeor flux due to eddy mixing. The hydrometeor field was adjusted accordingly. Details are described in Churchill (1988).

The model described above has limitations that result from the parameterizations used. Radiative transfer is sensitive to the size distribution and phase of hydrometeors and the crystalline structure of ice particles, but the model does not simulate this sensitivity. The model does not attempt to diagnose the explicit size distribution of hydrometeors. The microphysical parameterization was developed for temperatures considerably warmer than the tops of tropical cloud systems. Due to the dearth of in situ measurements in the tropical upper troposphere, this approach is the best possible at present. The simulations produce profiles of hydrometeors that are consistent with current observations; hence it is believed that the microphysical parameterizations are generally realistic. Although the current simulation reaches an altitude of only 13 km, a forthcoming paper will show similar results for a tropical Asia cloud simulation that reaches altitudes of 18 km with temperatures as low as −90°C (see also Churchill 1988).

3. Results of calculations

The role of radiation in the stratiform region of tropical cloud clusters is examined here with regard to three related questions: 1) To what extent is the precipitation of the stratiform region affected by radiation? 2) How strongly does radiation affect the diabatic heating profile of a cloud cluster when radiative transfer is treated consistently with the kinematics, microphysics, and thermodynamics of the stratiform region? 3) Does radiation affect the longevity of upper tropospheric cirrus clouds?

a. Model initialization, boundary conditions, and experimental design

As noted in section 1, the case examined in this study is the 12 September 1974 squall line described by Gamache and Houze (1982, 1983, 1985). The analyzed fields of Gamache and Houze (1985) were used as initial fields of wind, temperature, and humidity. These fields were also used as input by Rutledge (1986). This set of data is appropriate for a steady-state diagnostic study inasmuch as the winds are a composite over the mature stage of the stratiform region of a cloud cluster and are therefore representative of fairly steady-state conditions.

Rutledge and Houze (1987) pointed out that because of the low spatial resolution and smearing of the composite sounding-derived air motion field, the vertical motions in the forward part of the lower troposphere of the stratiform region are not accurately resolved, and that the diagnostic results of Rutledge (1986) are therefore not meaningful in this region. The present calculations are also affected by these spurious air motions. However, the effects of radiation and mixing are found to be most pronounced in the upper troposphere. Hence, errors in the lower troposphere composite vertical air motions do not affect the results of this study.

The present study uses a single two-dimensional slice in height and distance that passes from the front to the rear of the stratiform region of the composite squall line. The coordinate of this slice in the Gamache and Houze storm-relative frame of reference is $\beta = 25$ km. This particular slice was chosen because it exhibits well the mesoscale updraft (Fig. 5). The squall line is beyond the left side of the diagram, upwind and ahead of the stratiform region. The maximum updraft velocity in the stratiform region was 31 cm s^{-1} at 7.5 km altitude, while a mesoscale downdraft of 5 cm s^{-1} was present at low altitudes. The upward velocities below 4 km, located 0–100 km on the horizontal axis, are the spurious values mentioned above. Model simulations run with other slices of data from Gamache and Houze produced qualitatively similar results.

All hydrometeor categories were initially zero in the interior of the model. Along the left boundary of the model, where the convective line was located, hydrometeors were set and held constant, according to Fig. 6 (from Rutledge 1986), to simulate advection of hy-

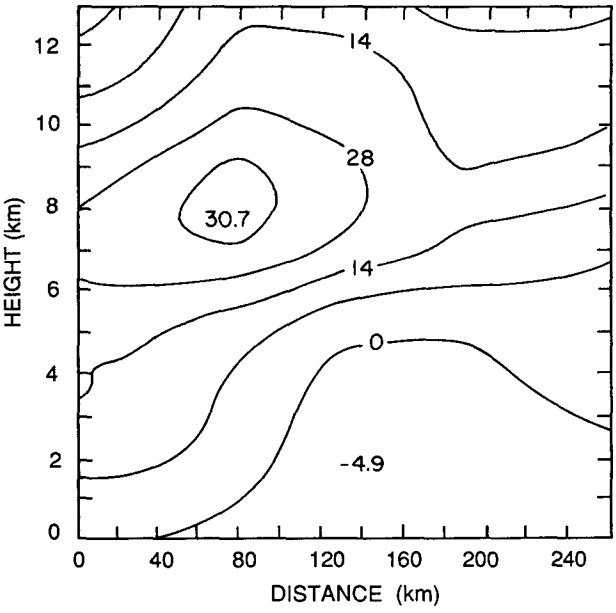

FIG. 5. Vertical wind speed (cm s^{-1}) for the GATE model simulations.

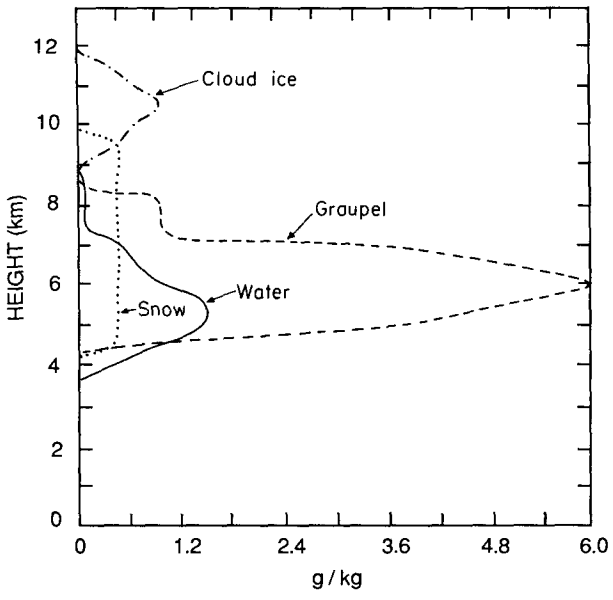

FIG. 6. Boundary profiles of hydrometeors advected into the model domain. From Rutledge (1986).

drometeors from convective cells. These values were predicted by an early version of the one-dimensional time-dependent convective cloud model of Ferrier and Houze (1989) using the 1200 UTC sounding from the ship *Oceanographer* on day 255 of GATE as input. The convective model was run with a microphysical scheme very similar to the one used in this study, predicting the mass of hydrometeors detrained from a convective cell. For further details on this model, see the dissertation of Ferrier (1987). The detrained masses implied by the model over the lifecycle of the cell were converted to mixing ratios by assuming that the hydrometeors were detrained into a horizontal area of 10^2 km^2 near the cell. The area used in arbitrary, but was chosen to represent the horizontal scale of a convective cell. This area produces hydrometeor mixing ratios near the cell that are reasonable. No observations exist that determine what the mixing ratios of hydrometeors advected into the stratiform region should be for tropical cloud clusters. The results, however, do not appear to be particularly sensitive to the mixing ratios advected into the stratiform region, except perhaps near cloud top, where radiative heating and cooling are most active. Along the right-hand model boundary the hydrometeor contents were initialized to zero. Inflow from the right-hand boundary in the lower troposphere thus advected clear air into the model domain. The temperature and water vapor fields were initialized along the left and right boundaries of the model using the Gamache and Houze data, and these boundaries were held constant.

Calculations for the two-dimensional stratiform region were carried out until steady-state conditions were obtained. Steady state was considered to have been attained numerically when the distribution of hydrometeors changed by about 0.01 g kg^{-1} on the time scale of an hour, and when the horizontally averaged tendency term of Eq. (1) was about 0.01 W kg^{-1}.

b. Control run

In the first model run described later, called the "control run," all radiation is turned off [term H_R in Eq. (1) was set to zero], but convective adjustment and cloud mixing are active. The horizontal storm-relative wind speeds used to initialize the control run are shown in Fig. 7. Horizontal relative winds up to 20 m s^{-1} blew from front to rear of the system in the upper troposphere, and rear-to-front inflow to 2.5 m s^{-1} occurred in the lower troposphere.

The steady-state hydrometeor fields obtained in the control run are shown in Fig. 8, where the mixing ratio of snow was about 0.15 g kg^{-1} at a horizontal distance of about 150 km and at an altitude of 9 km, and graupel extended horizontally about 170 km in the layer between 3 and 9 km. The graupel distribution appears to be realistic. Churchill and Houze (1984) reported heavily rimed ice particles at 8-km altitude in the stratiform region of a tropical cloud cluster extending over hundreds of kilometers. Rain, which extended from the surface to about 4 km, produced nearly saturated conditions toward the rear of the system, where the mesoscale downdraft was located (Fig. 1). Cloud ice was present from about 9 to 12.5 km, with maximum mixing ratio of about 0.3 g kg^{-1} at 12.5 km. Near cloud top, cloud-ice mixing ratios increased from deposition, but there was not enough mass to convert it to snow.

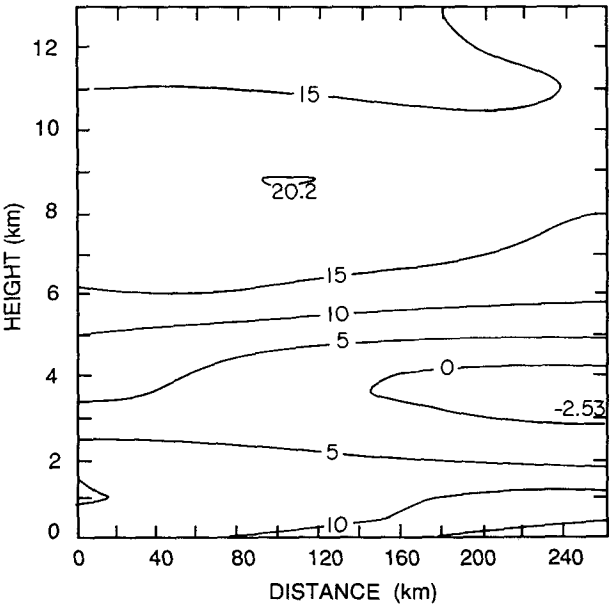

FIG. 7. Horizontal wind speed (m s^{-1}) for the control run. Positive values indicated motion from left to right.

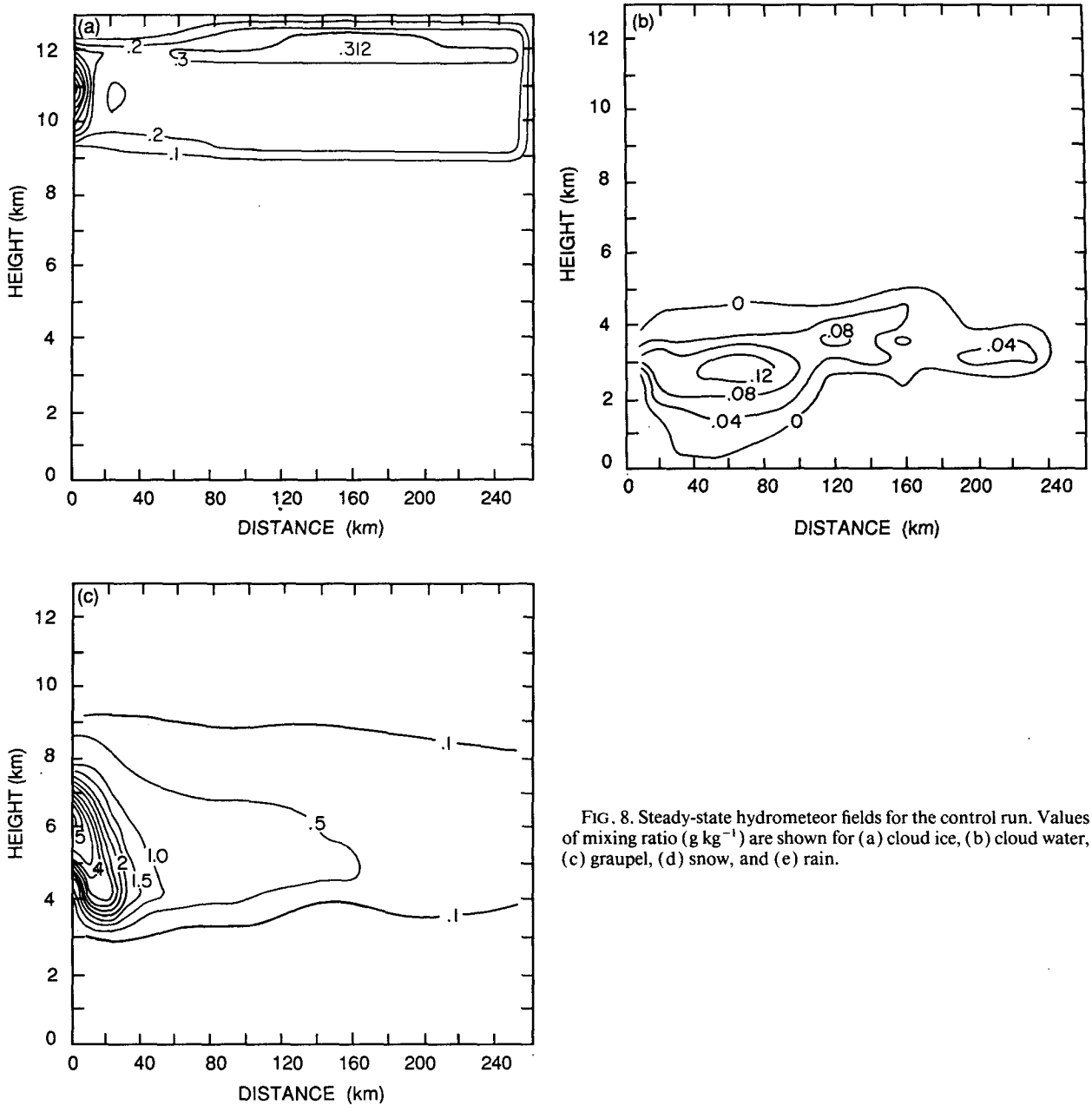

FIG. 8. Steady-state hydrometeor fields for the control run. Values of mixing ratio (g kg^{-1}) are shown for (a) cloud ice, (b) cloud water, (c) graupel, (d) snow, and (e) rain.

No sensitivity tests of various autoconversion thresholds and rates were made.

Figure 9a shows horizontally averged steady-state values of all the terms in the thermodynamic energy balance expressed in Eq. (1). Latent heat release nearly balanced the adiabatic cooling due to lifting, as expected in an atmosphere marginally stable to convection. In the upper troposphere positive horizontal temperature advection also offset the adiabatic cooling. The advection was positive because the temperature on the upwind boundary was held constant, while vertical motion led to cooling on the downwind side of the stratiform region. Cooling at 3–4 km, below the melting layer, was associated with evaporation (H_L) and caused convective overturning (H_E). At about 2.5 km, the cooling due to convective overturning was balanced by latent heat release from condensation. The resulting condensation produced model cloud water (Fig. 8b) that suggested the presence of stratus or fractostratus, such as is often observed in the lower troposphere beneath the stratiform regions of cloud clusters (e.g., Churchill and Houze 1984). To determine if the stratus was an artifact of the mesoscale vertical motion, the simulation was run again with the mesoscale updraft

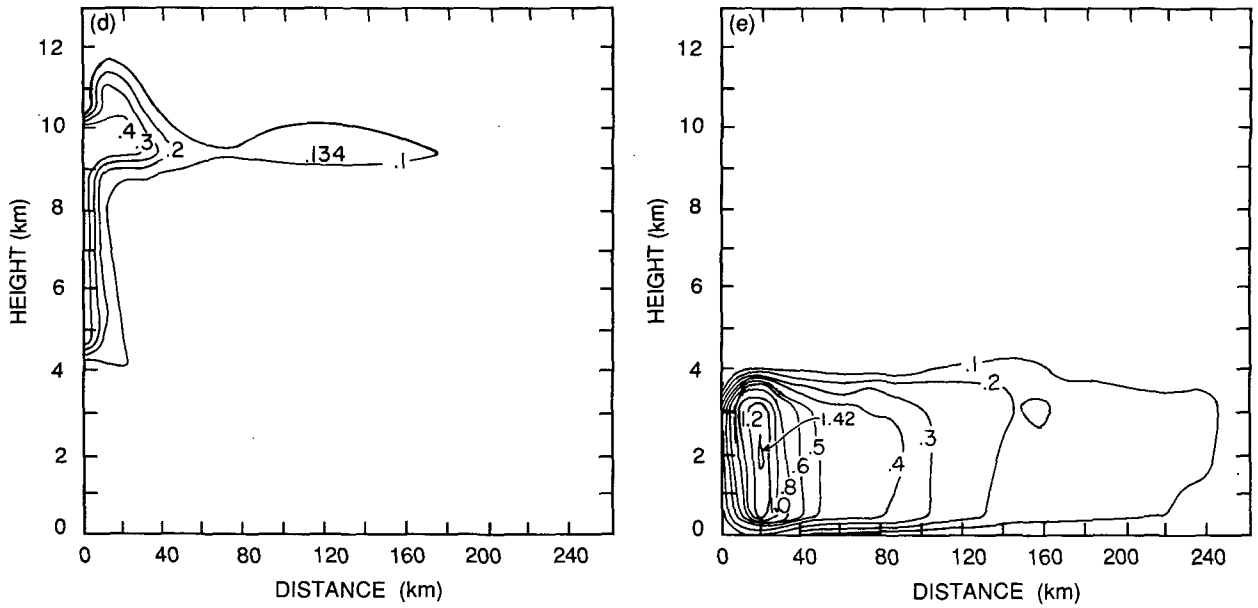

FIG. 8. (*continued*)

and downdraft turned off. Evaporation of precipitation advected from the model boundary still produced convective overturning, and fractostratus formed again, though in smaller amounts.

Figure 9b shows only the horizontally averaged diabatic heating terms for the control run (H_L and H_E), and Fig. 9c shows their sum ($H_L + H_E$). Latent heat release, associated with the mesoscale updraft, dominated the mid-to-upper troposphere. Between 1 and 4 km, melting and evaporation of precipitation caused cooling. Melting was dominant near the convective cell where large amounts of ice were present. Evaporation was dominant in the mesoscale downdraft region. The cooling due to melting was -0.4 W kg^{-1}, or about about 1.4° h^{-1}. This value is consistent with Leary and Houze (1979) who determined cooling rates due to melting of 1°–7° h^{-1} in a layer 1 km deep near the base of the cloud deck. In the model this cooling produced unstable lapse rates, which led to convective warming that offset the cooling near 2 km. The maximum diabatic cooling in the lower troposphere, when normalized by the average surface rainfall rate of 19 mm day^{-1}, yields a cooling rate of 0.65° day^{-1} per cm day^{-1} of surface rain. Houze (1989, Fig. 7) estimated cooling by evaporation in the lower troposphere in the mesoscale downdraft of 2° day^{-1} per cm day^{-1}. The mesoscale downdraft used in the present simulation had a maximum value of 5 cm s^{-1}, whereas Houze had a mean speed of 10 cm s^{-1}. The downdraft in this study, which may be underestimated owing to the spurious upward motion in the lower troposphere, accounts for the lower amount of cooling via evaporation.

In the upper troposphere, the peak latent heat release of about 0.6 W kg^{-1} corresponds to a maximum value of about 50° day^{-1}. The normalized latent heating is about 2.6° day^{-1} per cm day^{-1} of surface precipitation, which agrees closely with the results of Houze (1989, Fig. 7). The cooling due to evaporation between the surface and 2 km was 0.1 was 0.1 W kg^{-1} (about 8° day^{-1}), which is similar to Houze's estimate.

c. Nighttime simulation

To simulate nighttime conditions, longwave radiation was included, but not solar radiation. The horizontal and vertical winds and hydrometeors used in the control run were used again for this experiment, called "nighttime." The cloud ice, snow, graupel, and cloud water were identical, to within order 10^{-1} g kg^{-1}, to the values of the control run. Hence, the addition of infrared radiation and convective adjustment did not affect the hydrometeor fields. This demonstrates that the radiative destabilization does not influence the development of precipitation by acting directly on the stratiform cloud region. Any influence that radiation has on the stratiform region must be indirect, most likely through radiative effects on the clear-air environment, as suggested, for example, by Dudhia (1989). The energy balance, Fig. 10, shows that adiabatic cooling, still the most dominant term, has not changed from the control run from 4 to 13 km. The model was run both with and without rain incorporated in the pathlengths for radiative transfer, and no change in microphysical structure resulted. The infrared cooling, at 12.5 km, was about 0.4 W kg^{-1}, which is about 34° day^{-1}. The cloud top cooling did not change the microphysics, probably because there is inadequate supersaturation near cloud top to produce significant deposition.

Cooling due to radiative destabilization is evident from 11 to 11.5 km, just below the layer where cloud

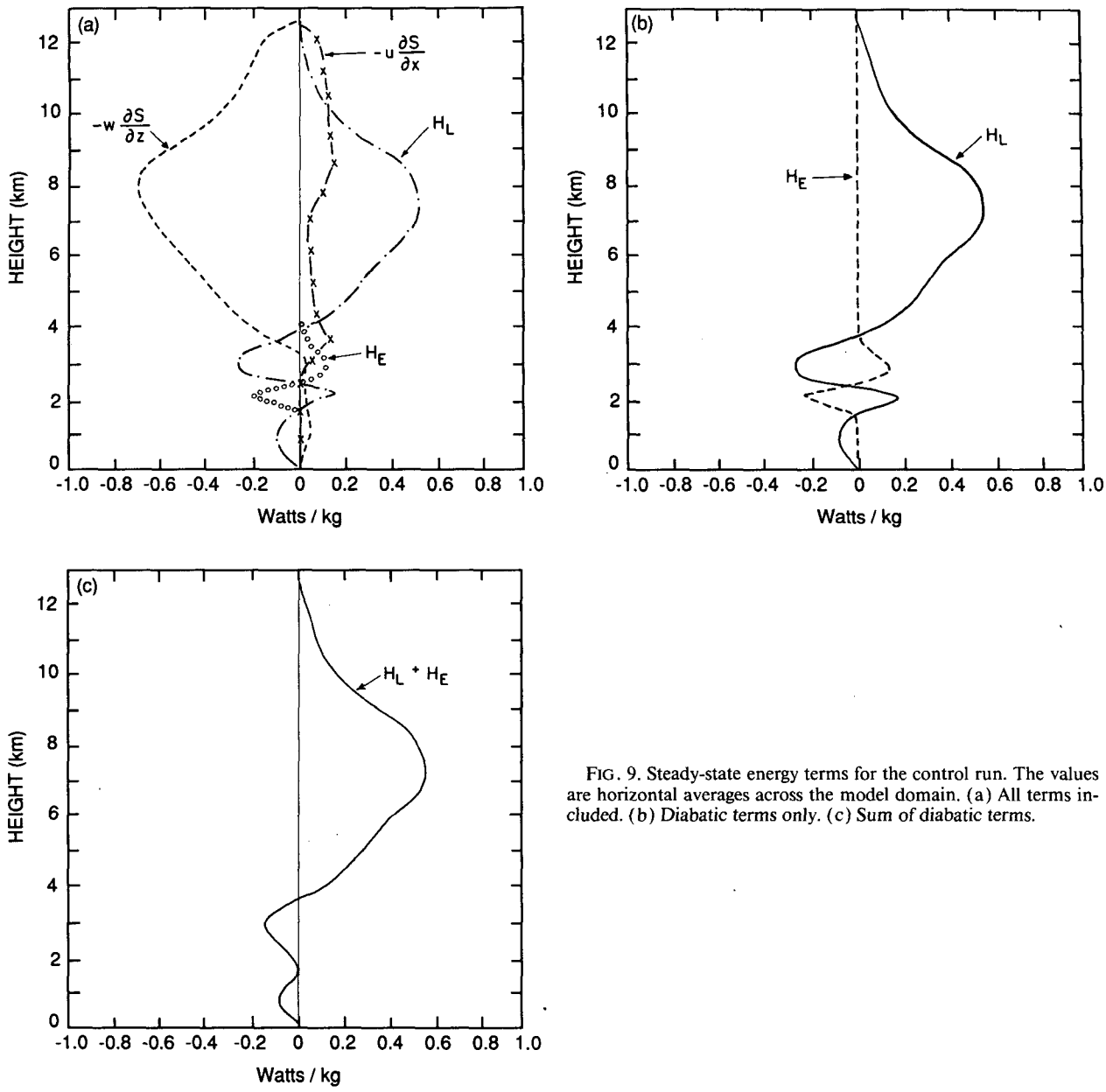

FIG. 9. Steady-state energy terms for the control run. The values are horizontal averages across the model domain. (a) All terms included. (b) Diabatic terms only. (c) Sum of diabatic terms.

is cooled radiatively, and convective heating is evident from 12 to 13 km. Overturning occurred in this region because the cooling at cloud top destabilized the upper portion of the cloud. The overturning balanced the infrared cooling partially. It is significant that radiative destabilization in the deep precipitating stratiform cloud behind the squall line was confined to a shallow, very high layer in this case. A future paper will show similar results in another tropical cloud cluster.

Horizontal temperature advection is greater between 10.5 and 12 km, compared with the control run, and it is as powerful as the convective overturning. The horizontal temperature advection is greater in this case because radiative cooling across the cloud top increased the horizontal temperature gradients. As hydrometeors flow toward the rear of the system near cloud top, they may spend several hours being exposed to radiative cooling; hence horizontal temperature gradients cloud be present near cloud top. Since regions of cold air near cloud top in the stratiform region of mesoscale systems have been observed in the midlatitudes (Fritsch and Maddox 1981) and in the tropics (Johnson and Kriete 1982), the temperature gradients in the present simulation may be realistic.

The lowest cloud top temperatures occurred downwind, where radiation had been acting the longest. The temperature upwind was warmer, where air advected across the boundary had been maintained in a ther-

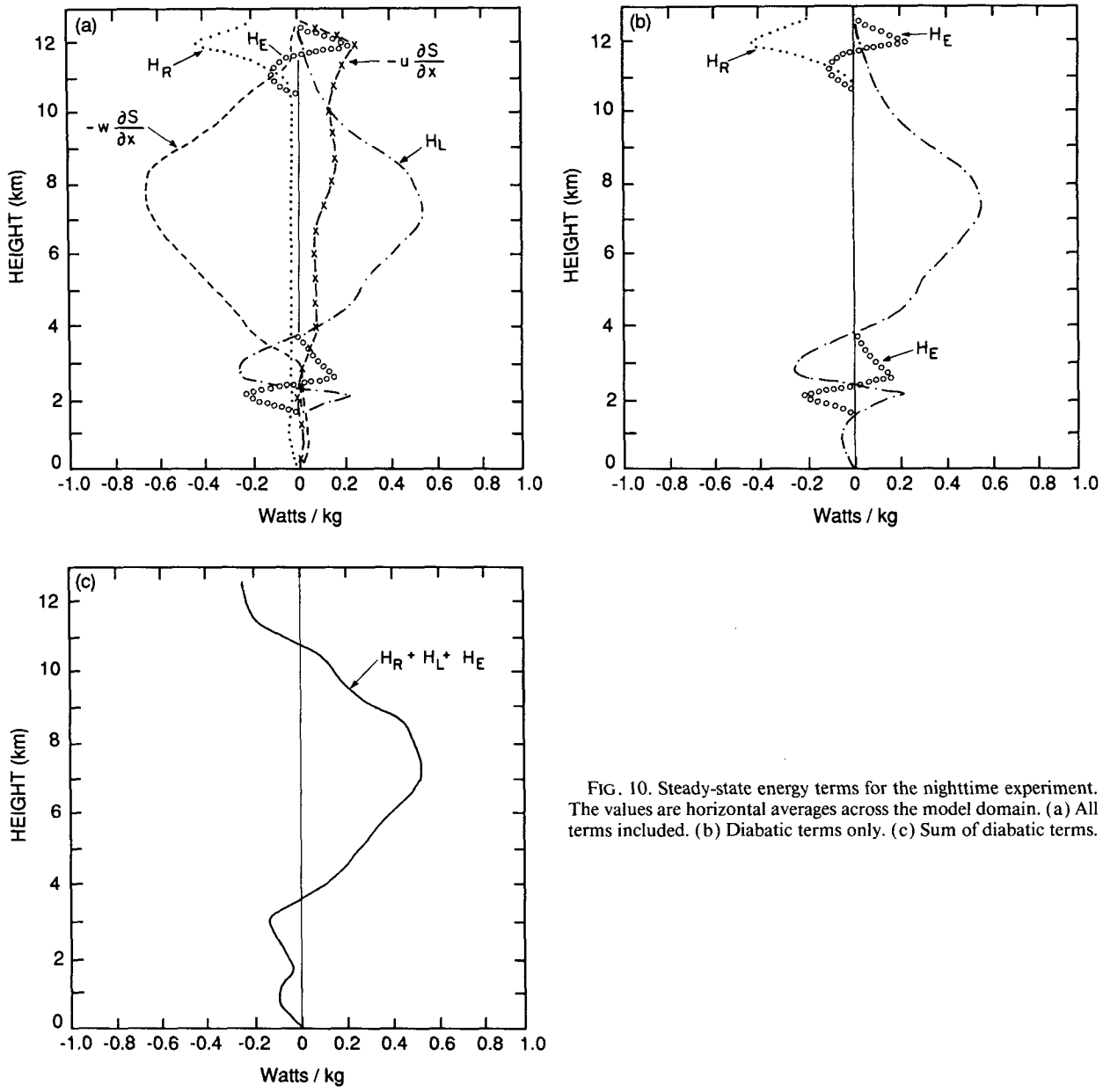

FIG. 10. Steady-state energy terms for the nighttime experiment. The values are horizontal averages across the model domain. (a) All terms included. (b) Diabatic terms only. (c) Sum of diabatic terms.

modynamic state corresponding to conditions assumed to hold in the convective region. The increased temperature gradient, however, owing to the cooling downwind, led to increased warming by horizontal advection. Thus a feedback occurs in which the radiative cooling leads to increased warming by advection in the model domain. The diabatic heating in the nighttime experiment (Fig. 10) was very similar to the values for the control run (Fig. 9), except near cloud top. Between 11 and 12.5 km, infrared cooling and convective adjustment produced net cooling. At 12 km the cooling rate was about 17° day^{-1}. When normalized by the surface precipitation rate, this nighttime cooling was about 0.9° day^{-1} per cm day^{-1} of surface precipitation.

d. Incipient anvil

Stages in the life cycle of a tropical cloud cluster have been presented in the form of conceptual models by Leary and Houze (1979), Houze et al. (1981), and Houze (1982). To simulate the development of an anvil cloud that is produced by hydrometeors detrained from convection alone, the model boundary was initialized with the same vertical profile of hydrometeors as before, the mesoscale updraft was turned off, and longwave radiation and convective adjustment were used. This experiment produced a cirriform cloud, of the type cirrostratus cumulonimobogenitus, as a plume extending downwind of the line of convective cells.

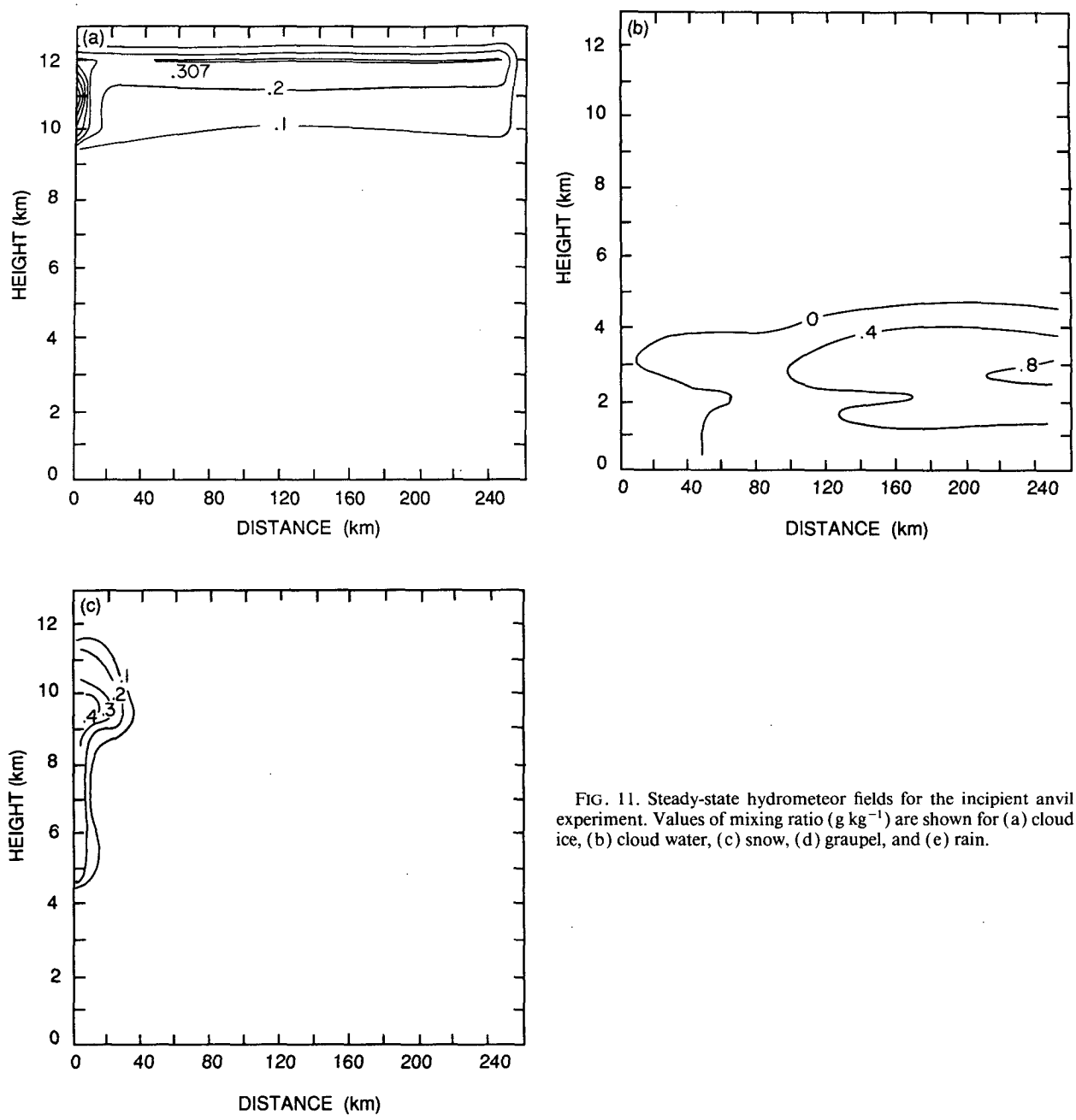

FIG. 11. Steady-state hydrometeor fields for the incipient anvil experiment. Values of mixing ratio (g kg^{-1}) are shown for (a) cloud ice, (b) cloud water, (c) snow, (d) graupel, and (e) rain.

Figure 11 shows the steady-state distribution of hydrometeors. No precipitation particles were formed in the anvil, and stratus formed in the lower troposphere (Fig. 11b). Cloud ice was horizontally distributed across the model domain, but with vertical variations extending from 9 to 12.5 km. The maximum mixing ratio, 0.3 g kg^{-1}, was near cloud top. The air near the anvil base was unsaturated due to heating by infrared radiation, and the lapse rate was close to dry adiabatic. At cloud top, infrared cooling kept the top of the cloud saturated, preventing sublimation. The lapse rates here were moist adiabatic. There was no increase in precipitation due to radiative destabilization of the cirrus.

This experiment suggests that cirrus clouds in the upper troposphere can remain for an extended period of time, and confirms they are active radiatively and convectively, thus indicating they may have a significant effect on the radiation budget of the earth. This result is consistent with the widespread, long-lived cirrus that is observed frequently in the tropics.

Since convective adjustment offset infrared heating at cloud base, and kept the cloudy air saturated, the

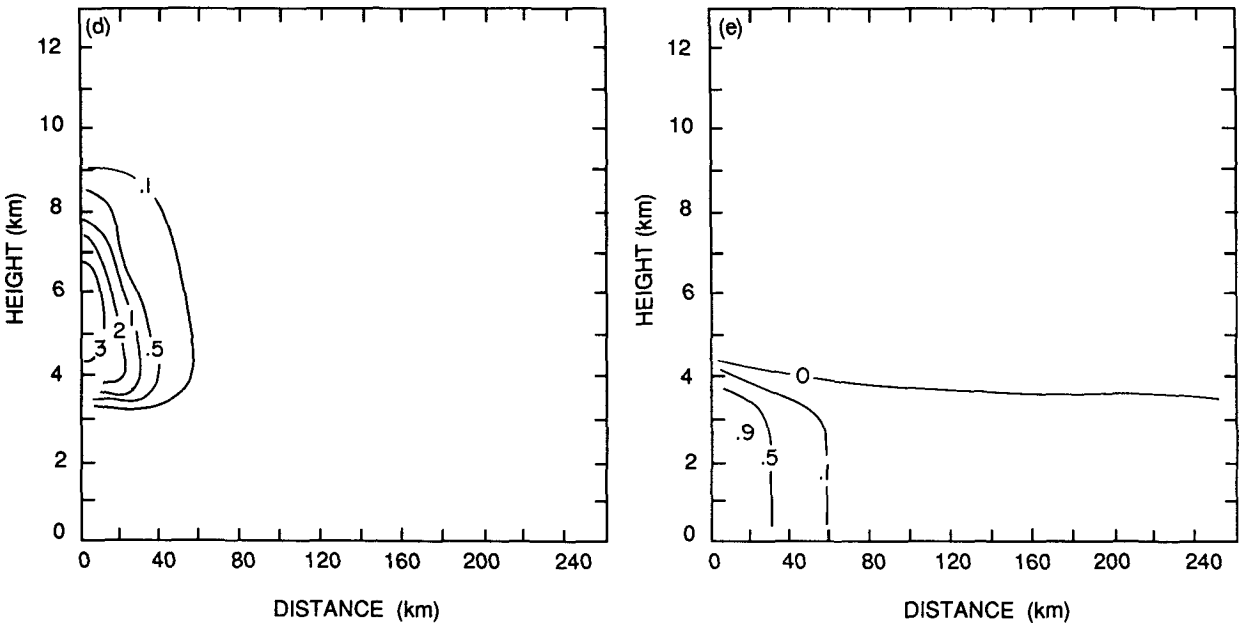

FIG. 11. (*continued*)

cloud could not sublimate. The cirrus cloud did not precipitate, likely because there were too many small ice particles at this height to allow precipitation to form.[2] The primary mechanism for reduction of cirrus clouds in the tropics could be three-dimensional dispersion of the cloud ice into subsaturated air by wind and background eddy mixing—processes not simulated in this study—followed by sublimation of the cloud-ice particles in subsaturated air.

The energy balance (Fig. 12) shows that infrared cooling at cloud top was offset by convective adjustment and warm air advection. The warm air advection from the convective cells seems reasonable, as discussed above. From 9 to 10 km, radiative heating at cloud base was balanced by convective adjustment. In the lower and middle troposphere, melting and evaporation cooled the air, and this was balanced by warm air advection. Between 2.5 and 4 km diabatic cooling was due primarily to melting and evaporation of hydrometeors near the upwind boundary.

e. Mixing of cloud water and ice

All the experiments described above were executed with vertical mixing of cloud ice and water included. Recall that only the nonprecipitating hydrometeors were mixed via diffusion, since precipitation was presumed to fall much more quickly than diffusion can move it.

Convective adjustment occurred typically in the layer from 9 km to 12.5 km, which encompassed most of the cloud ice. The amounts of cloud ice that were transported by eddy mixing over the duration of the experiments were much smaller than the cloud ice mixing ratios. The incipient anvil experiment, for example, showed eddy mixing through most of the cirrus cloud. Yet the rate of change in cloud ice due to eddy flux, integrated with respect to time over the run, was on the order of 10^{-3} g kg^{-1}. Since the cloud ice transport was an order of magnitude smaller than the absolute cloud-ice contents, eddy mixing of cloud ice had little effect on the vertical distribution of cloud ice content.

The results above, and also results from Rutledge (1986) who used no cloud-ice mixing, show that cloud-ice contents usually increase towards cloud top. Hence the diffusion of cloud ice was generally directed downward instead of upward, since the gradient favored downward diffusion of cloud ice, according to the parameterization used here.

f. Daytime simulations

To simulate daytime conditions, shortwave heating was turned on, so that all physical processes contained in the model were active. This experiment, called "daytime," differs from "nighttime" only by the addition of shortwave radiation.

The energy balance, Fig. 13a, shows that solar heating had maximum magnitude of 0.5 W kg^{-1}, similar in magnitude, but opposite in sign to the maximum infrared cooling. The shortwave heating, however, ex-

[2] Observations in clouds at the top of mesoscale systems over tropical Australia, obtained during the Stratosphere Troposphere Exchange Program (STEP) indicate that precipitation-sized ice particles were generally absent. The mean size of ice particles was about 20 μm, (L. Pfister and R. Knollenberg, personal communication). The simulations here are consistent with these observations.

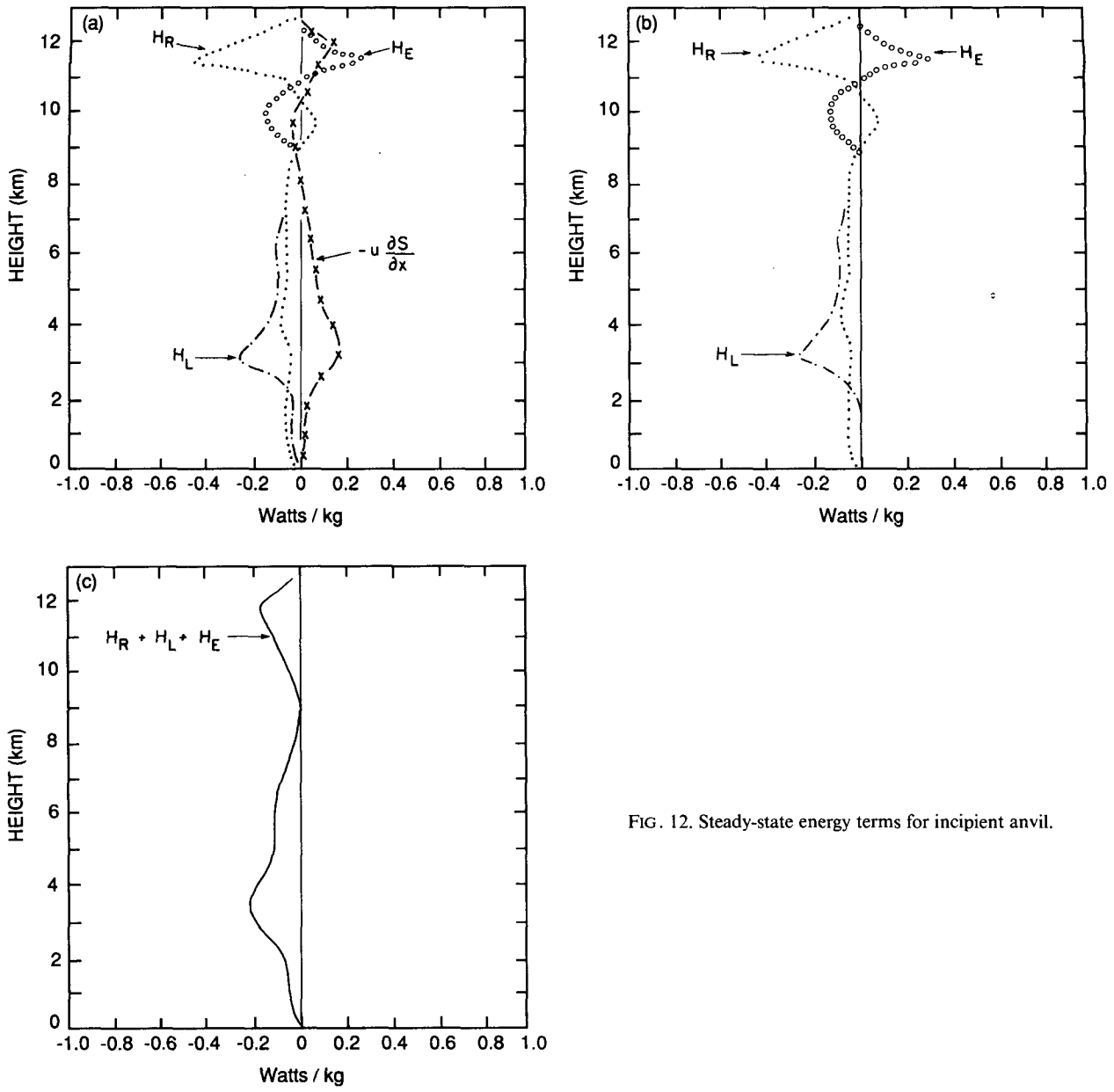

FIG. 12. Steady-state energy terms for incipient anvil.

tended down to about 9 km, thus heating a layer of cloud about 4 km thick. The peak magnitude of the convective adjustment was reduced from about 0.4 to 0.05 W kg^{-1}, compared to the nighttime experiment.

The diabatic terms (Figs. 13b,c) show that net diabatic cooling occurred near cloud top even in the presence of sunlight. Consequently radiative destabilization near cloud top continued during the daytime. In the mid-to-upper troposphere solar heating produced a relative maximum in total diabatic heating near 11 km. With the maximum at about 7 km due to latent heat release, a bimodal distribution of total diabatic heating was thus produced within the cloud. The net cooling at cloud top during the day was about 0.2° day^{-1} per cm day^{-1} of rain, which was similar in magnitude to Houze's (1989, Fig. 7) estimate of about 0.5° day^{-1} per cm day^{-1}. Hence Houze's estimated diabatic heating and cooling profiles in the mid-to-upper troposphere appear reasonable, and Houze's (1982) conclusion that radiative heating is not as large as latent heating is supported by this study. The melting and evaporation of precipitation below cloud base and the convective overturning there were not changed by the presence of sunlight.

Despite the changes in energy balance, the daytime two-dimensional distributions of hydrometeors changed by order 1% or less compared to the nighttime or the control runs. This illustrates that solar radiation,

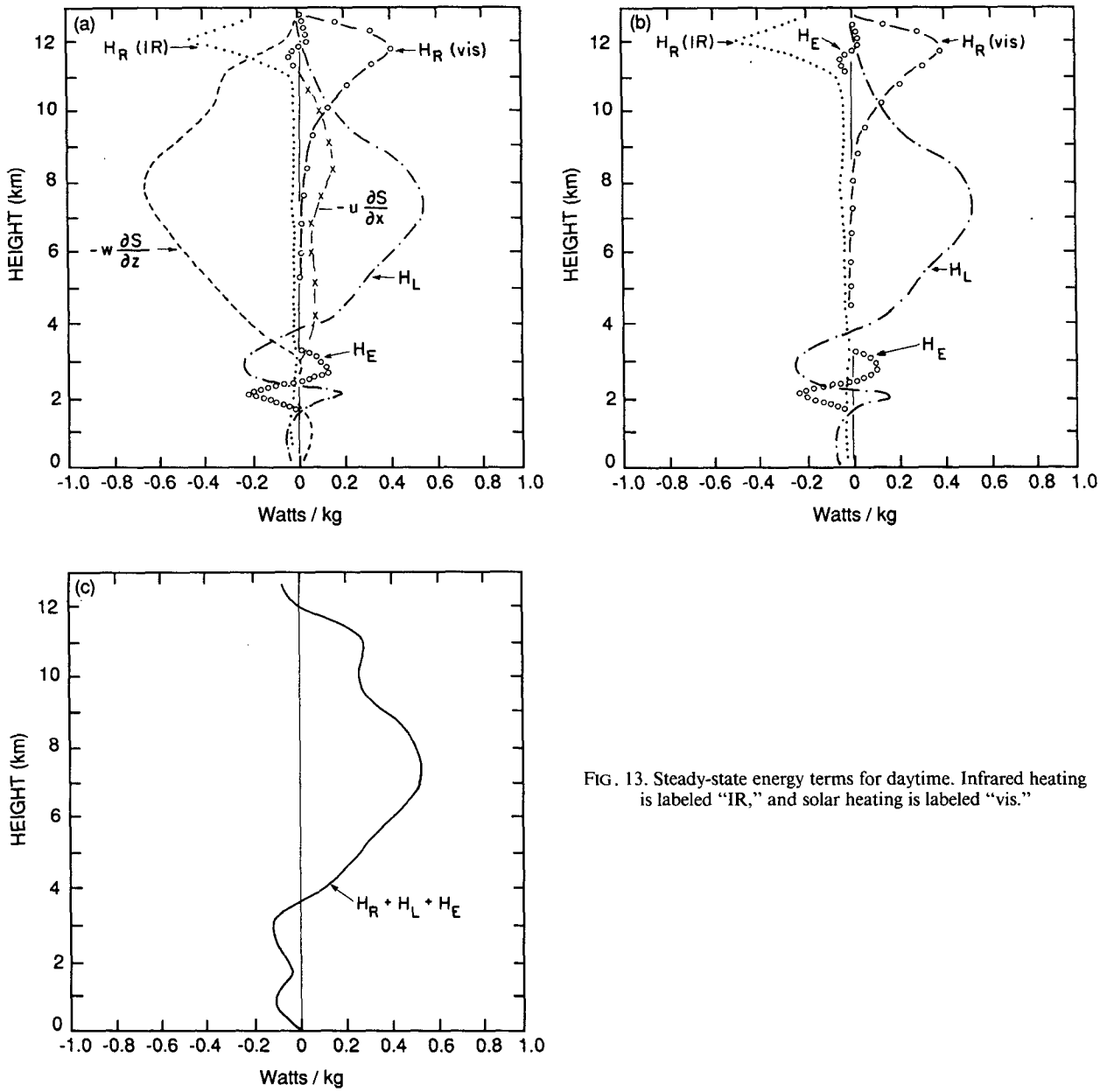

FIG. 13. Steady-state energy terms for daytime. Infrared heating is labeled "IR," and solar heating is labeled "vis."

like infrared, did not have a significant impact on the microphysical fields of the stratiform region of this squall line.

4. Conclusions

The goal of this study was to investigate the effects of radiation on the behavior of cloud clusters, excluding dynamical interactions. The specific objectives were to examine the direct effects of infrared and solar radiation on the water budget and steady-state energy balance of the precipitating stratiform region of a squall line and cirrostratus. These objectives were pursued using a hydrostatic, kinematic, mesoscale cloud model, incorporating parameterized turbulence, microphysics, and solar and infrared radiation. The steady-state hydrometeor and thermodynamic energy fields were diagnosed. Mixing ratios of cloud ice, snow, cloud water, rain, graupel, and water vapor were determined using bulk microphysical parameterizations. Horizontal and vertical motion were prescribed and held constant with respect to time during the simulations, no dynamical interactions were permitted, and convective adjustment was parameterized. Shortwave and longwave radiation were parameterized using a two-stream scheme that required as input vertical profiles of hydrometeor and water-vapor content, temperature, and pressure. Since the hydrometeor and thermodynamic fields are cal-

culated in the model, the radiation, microphysics, and turbulence are fully interactive. The model was initialized with thermodynamic fields and wind velocities diagnosed from a GATE squall line, and hydrometeors were advected from the adjacent convective region. The model was run until steady-state conditions were obtained.

In the top 1 km of the cloud system, infrared radiation from the cloud produced cooling. On the windward side of the cloud system, horizontal warm air advection balanced the infrared cooling. On the downwind side of the system, the cloud-top temperature decreased from radiative cooling until convective instability occurred. Near cloud top, convective adjustment transported water vapor and dry static energy upwards towards cloud top, balancing the radiative flux divergence.

The radiative destabilization was limited to a shallow layer near cloud top where water vapor mixing ratios were so low that little condensation occurred. Consequently radiative destabilization did not change the hydrometeor structure of the system, and infrared cooling and solar heating at cloud top had an insignificant effect on the hydrometeors.These results were not sensitive to whether or not rainfall was included in the radiative pathlengths; even with rainfall omitted from pathlengths, there was no change in hydrometeor mixing ratios. Since radiation did not change the hydrometeor fields of the stratiform region of this squall line, one can examine the water budget of the stratiform region ignoring the presence of radiative flux convergence. Hence the water budget results of similar studies (Gamache and Houze 1983; Rutledge and Houze 1987) are not diminished by the fact that they were carried out without radiation. The Webster and Stephens (1980) conjecture that radiative destabilization of the cloud layer may enhance the precipitation of the stratiform region was thus not supported by these experiments. Solar radiation warmed the top 3 km of cloud, but still allowed infrared cooling in the top 0.5 km of cloud to destabilize the cloud top. Radiative destabilization near cloud top continued even during the day. This inference is consistent with Lilly's (1988) theory of the cirrus outflow from cumulonimbus being maintained by radiative destabilization. It is concluded that radiation with fixed airflow does not affect the structure or water budget of the stratiform region.

Although the radiative effects do not change the water budget, the effects are indeed important in other ways. The lower troposphere was sensitive to radiative forcing. Clear-air cooling caused stratus to develop by night, indicating that the lower troposphere, which is conditionally unstable, is more sensitive to radiative destabilization than the upper troposphere. Beneath the base of the precipitating stratiform cloud deck, cooling due to melting and evaporation of hydrometeors caused convective instability. The resulting convective overturning produced some fractus or scud cloud.

Simulation of cirrostratus anvil in the upper troposphere, formed by detrainment of hydrometeors from a convective cell, shows that radiative destabilization maintained saturation in the cloud, but did not produce precipitation. This result suggests that thick cirrus clouds would have long lifetimes, and that radiation could be responsible for the longevity.

Acknowledgments. S. Rutledge provided a microphysical and kinematic program, K.-N Liou and S.-C. S. Ou provided a clear-air radiative program, J. Dudhia provided a helpful review, and K. Dewar drafted the figures. This research was supported by the National Aeronautics and Space Administration under Grant NAG 5-784.

APPENDIX

Model Details

a. In-cloud radiative transfer

The radiative transfer notation used here is similar to Stephens and Webster (1979). Radiative flux convergence is determined for each layer of each column in the model domain. Each layer is treated as if it were homogeneous in hydrometeor and gaseous content and a plane of infinite horizontal extent. In this manner, the model is divided into N discrete layers, enclosed by $N + 1$ levels (Fig. A1). In all equations and expressions that follow, positive superscripts by convention indicate radiation that is directed downward, and negative superscripts refer to upward-directed radiation.

For each layer n, reflectivity $\alpha(n)$, upward and downward transmissivities $\tau^{\pm}(n)$, absorptivity $A(n)$, and emissivities $\epsilon^{\pm}(n)$ are determined as functions of absorber pathlength for long- and shortwave radiation and as functions of solar zenith angle for shortwave radiation. For each level n one determines the upward and downward fluxes, $F^{+}(n)$ and $F^{-}(n)$, measured in watts per square meter (W m^{-2}). Source emission, $J^{\pm}(n)$, represents the emission from the adjacent layer n. The function $V^{\pm}(n)$ represents the total flux emitted and transmitted from all layers above level n, and all its multiple reflections from other layers. The computation of upward and downward fluxes requires values for the total reflectivity, α_T, for every level n, which represents multiple reflections from all layers above n. The downward radiative flux F^{+} at level n is determined from the recursion equation:

$$F^{+}(n) = \alpha_T(n)F^{-}(n) + V^{+}(n). \qquad \text{(A1)}$$

This states that the downward flux at level n equals the portion of the upward flux at level n that has been reflected downward from the sky above, plus the net downward flux due to emission from all layers above level n including its multiple reflections.

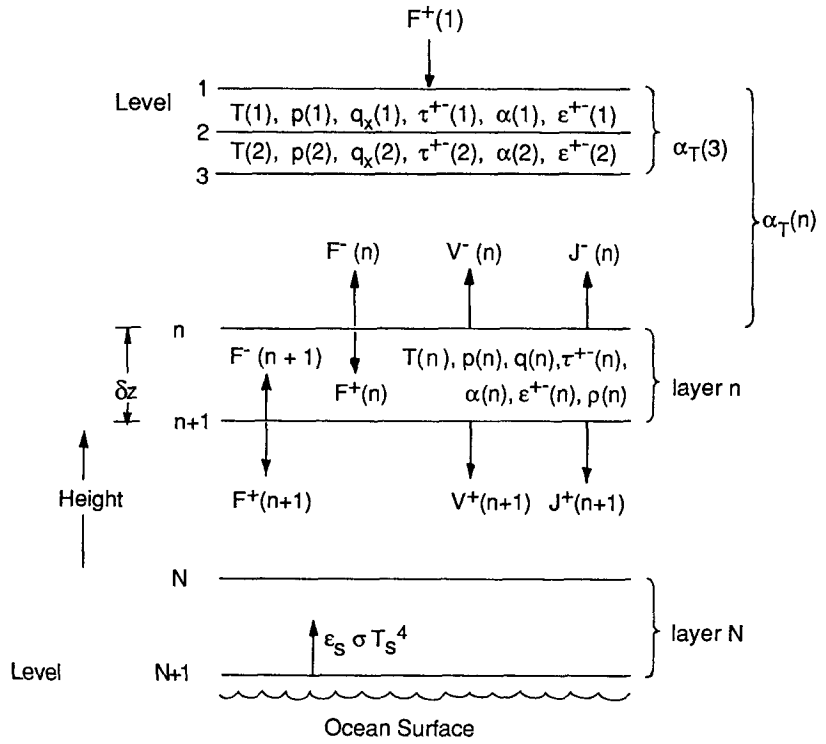

FIG. A1. The radiation model grid structure. Symbols are defined in the text.

The upward flux is given by

$$F^-(n) = \frac{\tau^-(n)F^-(n+1)}{[1 - \alpha_T(n)\alpha(n)]} + V^-(n),$$
$$n = 1, 2, \cdots, N. \quad \text{(A2)}$$

This states that the upward flux at level n equals the portion of the flux transmitted from level $n + 1$ including its multiple reflections plus the net upward flux due to emission from all layers above level $n + 1$ including multiple reflections.

Values for $\alpha_T(n)$, which represent the multiple reflections from all layers above level n, are determined recursively from

$$\alpha_T(n + 1) = \alpha(n) + \frac{\tau^+(n)\alpha_T(n)\tau^-(n)}{[1 - \alpha_T(n)\alpha(n)]}, \quad \text{(A3)}$$

assuming $\alpha_T(1) = 0$. The term $V^+(n)$ is determined recursively by:

$$V^+(n + 1) = \frac{\tau^+(n)V^+(n)}{[1 - \alpha_T(n)\alpha(n)]} + \frac{\tau^+(n)\alpha_T(n)J^-(n)}{[1 - \alpha_T(n)\alpha(n)]} + J^+(n + 1). \quad \text{(A4)}$$

Here $V^+(n + 1)$ is the total downward flux originating by emission in layers located above level $n + 1$ and all downward reflections thereof from layers above level $n + 1$. The first term on the right side of Eq. (A4) is the flux that enters layer n from above and is transmitted through the layer. The second term describes upwelling radiation emitted from layer n that is reflected from above and transmitted back down through the layer. The third is downward flux emitted from the layer itself.

The total upward flux originating by emission in layers located above level n and all its upward reflections constitute $V^-(n)$, which is given by

$$V^-(n) = \frac{\alpha(n)V^+(n)}{[1 - \alpha_T(n)\alpha(n)]} + \frac{J^-(n)}{[1 - \alpha_T(n)\alpha(n)]}. \quad \text{(A5)}$$

The first term contains all the upward reflections of $V^+(n)$ while the second term contains the upward emission from the layer itself, plus all its upward reflections.

The net radiative flux (W m^{-2}) at each level, defined as

$$\bar{F}(n) = F^-(n) - F^+(n), \quad \text{(A6)}$$

is related to heating, H_R(W kg^{-1}), in Eq. (1) by

$$H_R = \frac{1}{\rho}\frac{\partial \bar{F}}{\partial z}, \quad \text{(A7)}$$

where ρ is the density of air.

The radiative flux divergences were updated once every 100 s, based on the microphysical fields at that time. It is not necessary to recompute the divergences for every time step, since the heating rate varies more slowly than the microphysical parameters. This common technique, which reduced substantially the computer time used, altered the results of model runs insignificantly.

A nested grid with a vertical resolution of 50 m was used to compute the radiative fluxes and flux convergence. This grid improved the accuracy of the radiative computations, since the clouds simulated here are optically thick. The nested grid was incorporated by linearly interpolating profiles of pressure, temperature, water vapor, and hydrometeor mixing ratios to the nested grid. After the radiative flux convergence was determined on the nested grid, the fluxes were arithmetically averaged over 500 m to produce values that could be used in subsequent microphysical computations.

The computations of short- and longwave radiative fluxes require knowledge of the pathlengths of the absorbing medium, in mass per unit area, of each absorber. A pathlength, W, for an absorber, with mixing ratio q, was determined for each layer of the nested radiative domain by

$$W = \rho q \delta z \tag{A8}$$

where δz is the geometrical thickness of the absorbing layer (50 m). Sensitivity studies were made both with and without addition of rainfall to the liquid-water pathlengths, and no change in microphysical structure resulted. Generally snow, graupel and cloud ice, and cloud water were combined in the cloud liquid-water pathlength.

b. Longwave solutions in cloud

The source terms for layer n are

$$J^+(n+1) = \epsilon^+(n)\sigma T^4(n), \tag{A9}$$

and

$$J^-(n) = \epsilon^-(n)\sigma T^4(n), \tag{A10}$$

where upward and downward emissivities, $\epsilon^{\pm}$, are parameterized (see below) as a function of the pathlength of layer n. Temperature, $T(n)$, is provided by the solution of the thermodynamic equation of the kinematic model (Eq. 1), and σ is the Stephen–Boltzmann constant.

Boundary conditions for the infrared are that downward flux at the top of the model atmosphere is zero, so $F^+(1) = 0$; and upward flux from the surface is given by

$$F^-(N+1) = \epsilon_s \sigma T_s^4 \tag{A11}$$

where ϵ_s is the surface emissivity, which was set to 0.95, and the surface temperature, T_s, was set to 303 K, corresponding to a warm tropical ocean.

c. Parameterization of infrared cloud optics

Since in the steady-state cloud cluster, the most significant infrared flux divergence is near cloud top, where temperatures are well below −40°C, infrared optical parameters for cirrus cloud were used. Wiscombe (1983) notes that cirrus optical properties have much variability and that emissivities range from near zero in very thin, imperceptible cirrus to near unity in tropical cloud clusters.

The cirrus cloud emissivities, equal upward and downward, were obtained from the parameterization of Liou (1986), where

$$\epsilon = 1 - e^{-kW}, \tag{A12}$$

k was set to 0.029 and W is the hydrometeor pathlength (in g m^{-2}). Sensitivity tests were performed using values of 0.056, 0.06, and 0.08 for k, and qualitatively similar results were obtained.

The transmissivity for layer n, is determined then by:

$$\tau^{\pm}(n) = 1 - \epsilon^{\pm}(n) - \alpha(n). \tag{A13}$$

Reflectivity of infrared radiation by clouds was assumed zero. This assumption is appropriate to a steady-state cloud cluster that is black in the infrared, but may be incorrect for a thin cirrus cloud exposed to infrared radiation welling upward from the surface. Infrared reflectivity, which is only a few percent for cirrus clouds, was assumed to be zero. Hence, $\alpha(n) = \alpha_T(n) = 0$, and $\tau^{\pm}(n) = 1 - \epsilon^{\pm}(n)$ in the infrared only, and Eqs. (A1) and (A2) reduce to

$$F^+(n) = V^+(n) = \tau^+(n-1)F^+(n-1) + J^+(n) \tag{A14}$$

and

$$F^-(n) = \tau^-(n)F^-(n+1) + J^-(n). \tag{A15}$$

d. Shortwave solutions in cloud

Solar downward flux at the top of the atmosphere was taken to be, as in Stephens and Webster (1979), $F^+(1) = 1350$ W m^{-2} cosθ, where θ is the sun zenith angle. The zenith angle was assumed to be 60°. The lower boundary condition is determined from an assumed surface albedo, α_s, which was set to 0.05, corresponding to the reflectivity of a typical ocean surface when the sun is high in the sky. Other zenith angles were used with little qualitative difference except that the magnitude of solar heating increased the higher the sun was in the sky. Not unless the sun was close to the horizon did the solar reflectivity of clouds increase so much that solar heating was negligible.

The upward solar flux at the lower boundary is

$$F^{-}(N+1) = \frac{\alpha_s V^{+}(N)}{[1 - \alpha_s \alpha_T (N+1)]}, \quad \text{(A16)}$$

as in Grant and Hunt (1968).

Solar absorptivity and reflectivity in the visible were determined from Table 6 of Liou and Wittman (1979). This parameterization was originally intended for cirrus clouds. The model was tested using the values in that table, and later the absorption coefficients were scaled by 0.29 to produce better agreement with the results of Ackerman et al. (1988). Transmissivity was determined as the difference between unity and the sum of absorptivity and reflectivity for each layer of the nested grid. The model results were qualitatively the same using both the modified and original Liou and Wittman coefficients.

e. Convective adjustment

The first step in the adjustment process is to identify all unstable layers by comparing the lapse rate at each level against the dry adiabatic lapse rate, starting at the top of the model and descending to the surface. To adjust an unstable layer that has a bottom at height z_B and top at height z_T, the mean dry static energy, $\bar{S}$, was determined:

$$\bar{S} = \frac{1}{z_T - z_B} \int_{z_B}^{z_T} (C_p T + gz) dz. \quad \text{(A17)}$$

Then a revised temperature, $T_1(z)$, for the layer was obtained by

$$T_1(z) = (\bar{S} - gz)/C_p. \quad \text{(A18)}$$

After adjusting an unstable layer, the adjustment process was repeated for the same vertical profile, starting at the top of the model. It was not unusual for the adjustment of one unstable layer to produce an instability relative to the rest of the sounding. With sufficient iteration, the sounding became stable with loss or gain of dry static energy limited to truncation error. By processing every vertical profile in the horizontal, all absolute convective instabilities were removed from the model while conserving energy.

The moist adjustment scheme, which is similar to the dry convective adjustment, modifies vertical profiles of temperature and humidity to maintain moist neutral stability and saturation. A moist unstable layer was defined as two or more levels in a vertical profile that are saturated, and in which the moist static energy decreases with height between the levels. At subfreezing temperatures saturation mixing ratios with respect to ice were used. The top and bottom levels of unstable layers were located by searching from the top of the model downward. After finding a continuously unstable layer within the cloud with base at height z_B and top at height z_T, vertical profiles of temperature change, $\delta T(z)$, and water vapor mixing ratio change, $\delta q(z)$, were determined to produce a modified sounding that is saturated between z_B and z_T:

$$q(z) + \delta q(z) = q_{si}[T(z) + \delta T(z), p]. \quad \text{(A19)}$$

Here q_{si} is the saturation mixing ratio with respect to ice. This adjustment was made such that moist static energy was conserved:

$$\int_{z_B}^{z_T} [L\delta q(z) + C_p \delta T(z)] dz = 0, \quad \text{(A20)}$$

where L is latent heat of condensation. It is assumed that the adjustment process is instantaneous. Horizontal advection of moist static energy is ignored in the adjustment process, and it is assumed that no fluxes occur between stable and unstable layers.

These two equations, which determine the two unknowns $\delta q(z)$ and $\delta T(z)$, were solved simultaneously by iteration until $\delta T(z)$ changed by no more than 10^{-4} °. This threshold conserved energy to order 0.1 J per grid point and required only several iterations to attain.

Simultaneous solutions were obtained by determining the mean moist static energy, $\bar{H}$, for an unstable layer N levels thick:

$$\bar{H} = \frac{1}{Z_T - Z_B} \int_{Z_B}^{Z_T} [C_p T(z) + Lq_v(z) + gz] dz. \quad \text{(A21)}$$

Then for each level in the layer, a new temperature, T_1, was obtained such that

$$C_p T_1(z) + q_{si}[T_1(z), p] + gz = \bar{H}. \quad \text{(A22)}$$

Once T_1 is known, the new water vapor mixing ratio is

$$q_{v1} = q_{si}(T_1, p). \quad \text{(A23)}$$

The changes in the profile are

$$\delta q_v(z) = q_{v1}(z) - q_v(z), \quad \text{(A24a)}$$

$$\delta T(z) = T_1(z) - T(z), \quad \text{(A24b)}$$

and

$$\delta H(z) = C_p \delta T(z) + L\delta q_v(z). \quad \text{(A24c)}$$

This is related to Eq. (1) by

$$H_E(z) = \frac{\delta H(z)}{\delta t}. \quad \text{(A25)}$$

This process brings the unstable layer to saturation and produces a constant moist static energy within the layer after adjustment.

REFERENCES

Ackerman, T. P., K.-N. Liou, P. J. Valero and L. Pfister, 1988: Heating rates in tropical anvils. *J. Atmos. Sci.*, **45**, 1606–1623.

Chen, S., and W. R. Cotton, 1988: The sensitivity of a simulated extratropical mesoscale convective system to longwave radiation and ice-phase microphysics. *J. Atmos. Sci.*, **45,** 3897–3910.

Churchill, D. D., 1988: *Radiation, Turbulence and Microphysics in the Stratiform Region of Tropical Cloud Clusters.* Ph.D. thesis, University of Washington, Seattle, WA, 121 pp.

——, and R. A. Houze, Jr., 1984: Development and structure of winter monsoon cloud clusters on 10 December 1978. *J. Atmos. Sci.*, **41,** 933–960.

Dudhia, J., 1989: Numerical study of convection observed during The Winter Monsoon Experiment using a mesoscale two-dimensional model. *J. Atmos. Sci.*, **46,** 3077–3107.

Ferrier, B. S., 1987: *One-dimensional Time-dependent Modeling of Squall-line Convection.* Ph.D. Thesis, University of Washington, Seattle, 259 pp.

——, and R. A. Houze, Jr., 1989: One-dimensional time-dependent modeling of GATE cumulonimbus convection. *J. Atmos. Sci.*, **46,** 330–352.

Fritsch, J. M., and R. A. Maddox, 1981: Convectively driven mesoscale weather systems aloft. Part I: Observations. *J. Atmos. Sci.*, **20,** 9–18.

Gamache, J. F., and R. A. Houze, Jr., 1982: Mesoscale air motions associated with a tropical squall line. *Mon. Wea. Rev.*, **110,** 118–135.

——, and ——, 1983: Water budget of a mesoscale convective system in the tropics. *J. Atmos. Sci.*, **40,** 1835–1850.

——, and ——, 1985: Further analysis of the composite wind and thermodynamic structure of the 12 September GATE squall line. *Mon. Wea. Rev.*, **113,** 1241–1259.

Grant, I. P., and G. E. Hunt, 1968: Solution of radiative transfer problems in planetary atmospheres. *Icarus,* **9,** 526–534.

Houze, R. A., Jr., 1982: Cloud clusters and large-scale vertical motions in the tropics. *J. Meteor. Soc. Japan,* **60,** 396–410.

——, 1989: Observed structure of mesoscale convective systems and implications for large-scale heating. *Quart. J. Roy. Meteor. Soc.*, **115,** 425–461.

——, and A. K. Betts, 1981: Convection in GATE. *Rev. Geophys. Space Phys.*, **19,** 541–576.

——, and P. V. Hobbs, 1982: Organization and structure of precipitating cloud systems. *Adv. Geophys.*, **41,** 3405–3411.

Johnson, R. H., and R. A. Houze, Jr., 1987: Precipitation cloud systems of the Asian monsoon. *Monsoon Meteorology,* C.-P. Cheng and T. N. Krishnamurti, Eds., Oxford University Press, 298–353.

——, and D. C. Kriete, 1982: Vertical motion of near-equatorial winter monsoon convection. *J. Meteor. Soc. Japan,* **43,** 1152–1163.

Leary, C. A., and R. A. Houze, Jr., 1979: Melting and evaporation of hydrometeors in precipitation from the anvil clouds of deep tropical mesoscale convection. *J. Atmos. Sci.*, **36,** 669–679.

Lilly, D. K., 1988: Cirrus outflow dynamics. *J. Atmos. Sci.*, **45,** 1594–1605.

Lin, Y.-L., R. D. Farley and H. D. Orville, 1983: Bulk parameterization of the snow field in a cloud model. *J. Climate Appl. Meteor.*, **22,** 1065–1092.

Liou, K.-N., 1986: Influence of cirrus clouds on weather and climate processes: A global perspective. *Mon. Wea. Rev.*, **114,** 1167–1199.

——, and S. Sasamori, 1975: On the transfer of solar radiation in aerosol atmospheres. *J. Atmos. Sci.*, **32,** 2166–2177.

——, and S.-C. S. Ou, 1981: Parameterization of infrared radiative transfer in cloudy atmospheres. *J. Atmos. Sci.*, **38,** 2707–2716.

——, and G. D. Wittman, 1979: Parameterization of the radiative properties of clouds. *J. Atmos. Sci.*, **36,** 1261–1273.

Manabe, J., S. Smagorinsky and R. F. Strickler, 1965: Simulated climatology of a general circulation model with a hydrologic cycle. *Mon. Wea. Rev.*, **93,** 769–798.

Rutledge, S. A., 1986; A diagnostic modeling study of the stratiform region associated with a tropical squall line. *J. Atmos. Sci.*, **43,** 1356–1377.

——, and P. V. Hobbs, 1983: The mesoscale and microscale structure and organization of clouds and precipitation in midlatitude cyclones. VIII: A model for the "seeder-feeder" process in warm-frontal rainbands. *J. Atmos. Sci.*, **40,** 1185–1206.

——, and ——, 1984: The mesoscale and microscale structure and organization of clouds and precipitation in midlatitude cyclones. XII: A diagnostic modeling study of precipitation development in narrow cold-frontal rainbands. *J. Atmos. Sci.*, **41,** 2949–2972.

——, and R. A. Houze, Jr., 1987: A diagnostic modeling study of the trailing stratiform region of a midlatitude squall line. *J. Atmos. Sci.*, **44,** 2640–2656.

Stephens, G. L., 1984: The parameterization of radiation for numerical weather prediction and climate models. *Mon. Wea. Rev.*, **112,** 826–867.

——, and P. J. Webster, 1979: Sensitivity of radiative forcing to variable cloud and moisture. *J. Atmos. Sci.*, **36,** 1542–1556.

Webster, P. J., and G. L. Stephens, 1980: Tropical upper-tropospheric extended clouds: Inferences from Winter MONEX. *J. Atmos. Sci.*, **37,** 1521–1541.

Wiscombe, W., 1983: Atmospheric radiation: 1975–1983. *Rev. Geophy. Space Phys.*, **21,** 997–1021.